Rev. Adv. Mater. Sci. 48 (2017) 131-141

PLASTIC DEFORMATION THROUGH STRESS-INDUCED MIGRATION OF HIGH-ANGLE GRAIN BOUNDARIES IN METAL-GRAPHENE NANOCOMPOSITES

S.V. Bobylev[1,2,3], N.F. Morozov[1,2,3] and I.A. Ovid'ko[1,2,3]

[1]Peter the Great St. Petersburg Polytechnic University, St. Petersburg 195251, Russia
[2]St. Petersburg State University, St. Petersburg 199034, Russia
[3]Institute of Problems of Mechanical Engineering, Russian Academy of Sciences, St. Petersburg 199178, Russia

Received: November 01, 2016

Abstract. A theoretical model is suggested which describes plastic flow through stress-driven migration of high-angle grain boundaries (GBs) in metal-graphene nanocomposites. In the framework of the suggested model, stress-driven GB migration gives rise to the formation of wedge disclinations at GB junctions and edges of graphene inclusions. Energy and stress characteristics of stress-driven GB migration are calculated in several metals (aluminium, nickel and Gum metal). It is found that graphene inclusions strengthen metal-graphene nanocomposites. This is well consistent with experimental data reported in literature. Also, it is revealed that graphene inclusions in metal-graphene nanocomposites either hamper or enhance unstable GB migration and thereby grain growth driven by stress, depending on inclusion length.

1. INTRODUCTION

Nanostructured metallic materials exhibit the excellent mechanical properties (superior strength, etc.) due to their specific structural features including ultra-small grain sizes and very large quantities of GBs; see, e.g., [1-17]. With these structural features, GB-assisted and -mediated deformation micromechanisms effectively contribute to plastic flow in nanostructured metals. Among such micromechanisms, of particular interest is the stress-driven GB migration that not only mediates plastic deformation, but also changes (increases) grain size [18-47]. As a corollary, operation of stress-driven GB migration in a metal during its plastic deformation can modify its properties sensitive to grain size.

Recently, a rapidly growing interest has been devoted to metal-matrix nanocomposites with nanoinclusions of graphene – a 2D carbon material with the unique mechanical properties [48-50] – being utilized as reinforcing fillers; see, e.g., [51-63]. These metal-graphene nanocomposites typically have coarse-grained metal matrices and demonstrate the outstanding mechanical characteristics such as high strength and Young modulus. In doing so, graphene nanoinclusions enhance strength of such nanocomposites owing to the three key factors: first, graphene stops lattice dislocations – basic carriers of plastic flow in metals – in nanocompo-

Corresponding author: Sergey Bobylev, e-mail: bobylev.s@gmail.com

sites during their mechanical loading; second, the stress transfer from a soft metal matrix to super-strong graphene nanofillers occurs; and, third, graphene nanoinclusions hamper both GB migration and thereby grain growth in nanocomposites during their synthesis involving mechanical and thermal treatment [58]. With the third factor, a metal matrix of a nanocomposite containing graphene has lower grain size, as compared to its unreinforced counterpart (pure metal fabricated under the same conditions). In its turn, strength s of metals increases with decreasing an average grain size $\langle d \rangle$ in accordance with Hall-Petch relation ($\sigma=\sigma_0+k\langle d \rangle^{-1/2}$), with k being the material constant parameter; see, e.g., [7,14]) so that nanocomposites are stronger than their pure metallic counterparts.

Micromechanism(s) and characteristics of hampering effects exerted by graphene nanoinclusions on GB migration are unknown. At the same time, their knowledge is of crucial importance for control and design of grain size in metal-graphene nanocomposites and thereby for enhancement in strength exhibited by such nanocomposites. Of utmost interest are the specific features of stress-driven GB migration in metal-graphene nanocomposites having nanostructured metal matrices; see, e.g., [63]. The main aim of this paper is to elaborate (briefly considered earlier [64]) theoretical description of stress-driven GB migration – a process dramatically influencing grain size – in metal-graphene nanocomposites. In doing so, we will theoretically examine stress-driven GB migration in nanocomposites with aluminum, nickel and Gum-metal matrices.

2. STRESS-DRIVEN MIGRATION OF GRAIN BOUNDARIES IN METAL-GRAPHENE NANOCOMPOSITES: GEOMETRIC ASPECTS

Graphene nanoinclusions are typically located at GBs of metal matrices in metal-graphene nanocomposites; see review [58] and references therein. In this context, we will focus our theoretical examination on stress-driven GB migration in metal-matrix nanocomposites containing graphene nanoinclusions at GBs. Let us consider a two-dimensional model of a metal-graphene nanocomposite specimen which is under tensile stress σ that initiates plastic flow (Fig. 1). In the framework of our model, plastic deformation involves stress-driven migration of the GB AB at which the graphene nanoinclusion is located (Figs. 1b and 1c). The GB AD is assumed to be a symmetric high-angle tilt boundary specified by tilt misorientation angle θ. The graphene nanoinclusion represents a few-layer graphene nanoplatelet that has thickness of 1-2 nm (a red rectangle in Fig. 1b) and is located at the fragment BC of the GB AD, as shown in Fig. 1b. When the shear stress τ is applied, the GB AD can migrate and thus mediate plastic flow.

In general, GB migration in a metal occurs through atomic re-arrangements at the GB and in its vicinities in adjacent grain interiors. Such re-arrangements are suppressed by immobile graphene nanoinclusions – metal atoms cannot move across graphene nanoplatelets – which thereby hamper the migration process. In this case, stress-driven migration of the GB AD hampered by the graphene nanoinclusion occurs as schematically shown in Figs. 1b and 1c. As to details, in the framework of our model, the fragment BC of the GB AD is immobile (due to the presence of the immobile graphene nanoplatelet), whereas the GB fragments AB and CD migrate to their new positions A'B' and C'D', respectively (Fig. 1c). Note that, in our early model [64] addressing GB migration hampered by a graphene nanoinclusion, we examined a simplified situation where the GB fragments AB and CD simultaneously migrate over the same distance. However, it is too limiting condition for real GB configurations. Therefore, here we will consider the situation where the GB fragments AB and CD can migrate over different distances l_1 and l_2, respectively (Fig. 1c).

We now specify other geometric parameters of the system under consideration. Let $2a$ be the length of the GB fragment BC (Fig. 1b), h denotes the distance between D and middle point of the nanoinclusion, and d is the length of the GB AD (Fig. 1b).

Stress-driven migration of the high-angle GB AD gives rise to the formation of new GB fragments BB' and CC' (Fig. 1b). Besides, for geometric reasons, stress-driven GB migration is accompanied by formation of wedge disclinations at GB junctions [66]. Let us examine this aspect in detail. In the case under consideration, we assume that GB junctions A and D in the initial state of the system (Fig. 1b) are geometrically compensated. That is, each of these junctions is characterized by the zero sum of misorientation angles specifying GBs adjacent to the junction; for details, see [65]. This, in particular, means that GB junctions do not create intermediate- and long-range stresses.

Stress-driven migration of the GB AD (Figs. 1b and 1c) violates balance of GB misorientation angles at pre-existent and new GB junctions A, B, C, D, A', B', C' and D' so that these junctions contain wedge disclinations (triangles in Fig. 1c) serving as powerful stress sources. More precisely, two disclination quadrupoles AA'B'B and CC'D'D are formed that consist of disclinations having strengths $\pm\omega$, where the strength magnitude ω is equal to tilt misorien-tation θ specifying the GB AD. Thus, all the disclinations shown in Fig. 1c have the same strength magnitude ω: disclinations with positive and negative strengths ω and $-\omega$, respectively, are shown as full and open triangles, respectively.

3. STRESS-DRIVEN MIGRATION OF GRAIN BOUNDARIES IN METAL-GRAPHENE AND GUM-METAL-GRAPHENE NANOCOMPOSITES: ENERGY AND STRESS CHARACTERISTICS

We now examine energy and stress characteristics of stress-driven GB migration in metal-graphene nanocomposites (Fig. 1). First, let us calculate the energy change ΔW that characterizes the migration transformation presented in Figs. 1b and 1c. Since defects are absent in the initial state of the system (Fig. 1b), the energy change ΔW has the five terms:

$$\Delta W = W_{AA'B'B} + W_{CC'D'D} + W_{int} + \Delta W_{gb} - A_{pl}. \quad (1)$$

Here $W_{AA'B'B}$ and $W_{CC'D'D}$ are the proper energies of the disclination quadrupoles AA'B'B and CC'D'D, respectively; W_{int} is the energy that specifies the elastic interaction between the disclination quadrupoles; ΔW_{gb} is the change in the GB energy due to the formation of the new GB fragments BB' and CC'; and A_{pl} is the plastic deformation work.

The first, second and third terms on the right-hand side of formula (1) are given by the expressions well known in the theory of disclinations in solids [66]. With these expressions, after some algebra, we have:

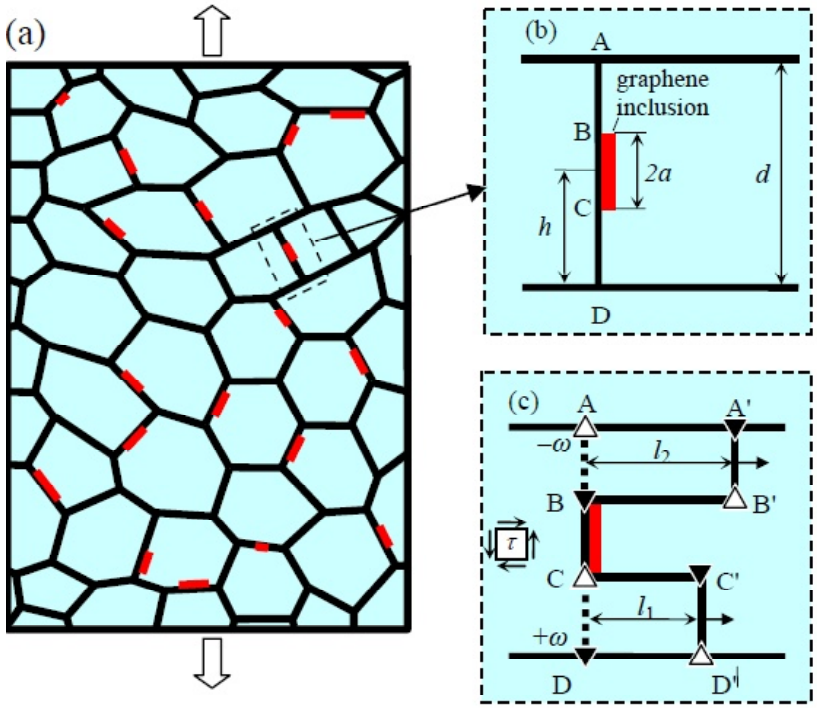

Fig. 1. Stress-driven migration of high-angle grain boundary in metal-graphene nanocomposite (schematically). (a) Nanostructured metal-matrix nanocomposite containing graphene nanoinclusions (red elongated rectangles) at grain boundaries (two-dimensional general view). (b) Nanocomposite fragment contains high-angle symmetric tilt boundary AD. Graphene nanoinclusion (red elongated rectangle) is located at this grain boundary. (c) Grain boundary AD migrates under stress to a new position A'B'BCC'D'. The migration process gives rise to the formation of two disclination quadrupoles AA'B'B and CC'D'D (for details, see text).

$$
\begin{aligned}
&W_{AA'B'B} + W_{CC'D'D} + W_{int} = \\
&D\omega^2 \big[2(f(l_1, h-a, 0) + f(h-a, l_1, 0) + \\
&f(l_2, d-h-a, 0) + f(h-a, l_1, 0)) \\
&-f(h+a, l_2, 0) + f(d, l_2, 0) - f(d, l_1 - l_2, l_1) + \\
&f(h+a, l_1 - l_2, l_1) - f(l_2, d-h+a, d) \\
&+f(l_2, 2a, h+a) - f(l_1, d-h+a, d) + \\
&f(l_1, 2a, h+a) - f(d-h+a, l_2, 0) + f(2a, l_2, 0) \\
&+f(d-h+a, l_1 - l_2, l_1) - f(2a, l_1 - l_2, l_1)\big],
\end{aligned}
\tag{2}
$$

where $f(x,y,z)=x^2\ln[(x^2+y^2)/(x^2+z^2)]$, $D=G/[2\pi(1-\nu)]$, G is the shear modulus, and ν is the Poisson ratio. The change in the GB energy due to the formation of the new GB fragments BB' and CC' is evidently related to their sum length l_1+l_2 as follows:

$$\Delta W_{gb} = \gamma(l_1 + l_2)\,, \tag{3}$$

where γ is the specific (per unit area) surface energy of the GBs. The work A_{pl} spent by the applied shear stress τ on movement of the GB fragments AB and CD over the migration distances l_1 and l_2, respectively (Fig. 1c), is given as:

$$A_{pl} = \tau\omega[l_1(h-a) + l_2(d-h-a)]\,. \tag{4}$$

Formulas (1)–(4) allow us to calculate the energy change ΔW that characterizes stress-driven migration of the GB AD (Figs. 1b and 1c). We calculated ΔW in the exemplary case of aluminum(Al)-graphene nanocomposite with Al matrix specified by the following values of material parameters: G=26.5 GPa, ν=0.34 [66], and γ=0.4 J/m^2 [67]. Note that, generally speaking, the specific energy of a high-angle GB depends on its misorientation. However, in many metals, including Al, the GB energy as a function of GB misorientation is approximately constant, except for narrow ranges of misorientation angles at and near angles corresponding to special GBs [69]. As a corollary, our approximation of constant γ =0.4 J/m^2 is good enough.

Fig. 2 demonstrates typical dependences $\Delta W(l_1,l_2)$ in the form of maps calculated for d=50 nm, ω=0.5, h=0.4d, a=0.1d and various values of the applied shear stress $\tau/D\omega$=0.01, 0.6, and 0.9 (Figs. 2a, 2b, and 2c, respectively), where $D=G/[2\pi(1-\nu)]$. It is seen that, for low values of the applied stress (Fig. 2a), the energy $\Delta W(l_1,l_2)$ monotonously grow with rising l_1 and/or l_2, that is, stress-driven GB migration is energetically unfavorable. For intermediate values of t, a local minimum (point M in Fig. 2b) appears at the map $\Delta W(l_1,l_2)$. That is, stress-driven migration of GB fragments AB and CD over some limited (equilibrium) distances becomes energetically permitted. In doing so, the local energy minimum corresponds to the equilibrium migration distances l_{e1} and l_{e2}. For high stresses, the energy $\Delta W(l_1,l_2)$ monotonously decreases with rising l_1 and/or l_2 (Fig. 2c), that is, stress-driven GB migration is unstable. It occurs as an energetically favorable process until at least one of the migrating GB fragments, AB or CD, is stopped at some structural obstacle, say, another GB.

The energy maps specifying Al have a rather character: similar maps are typical for many other metals. For shortness, we will not present such maps for other metals. At the same time, we will use such maps for Ni and Gum metals in our theoretical consideration in the rest of this paper.

With analysis of the energy maps $\Delta W(l_1,l_2)$, one can obtain dependences of the equilibrium migration distances l_{e1} and l_{e2} on various parameters of the system examined; see, e.g., Figs. 3 and 4, for Al-graphene and nickel(Ni)-graphene composites, respectively. (In calculations of dependences in Fig. 4, we used the following values of parameters characterizing Ni: G=76 GPa, ν =0.31 [66] and τ=1.6 J/m^2 [69]. These figures, in particular, demonstrate difference between the migration distances l_{e1} and l_{e2} (in contrast to the assumption in our early model [64]).

Figs. 3a and 4a present typical dependences of the migration distances on the applied stress. These dependences show growth of the migration distances with rising the applied stress and transition to the unstable migration regime at some critical values (τ_{c2}) of the stress. The dependences of l_{e1} and l_{e2} on the parameter h specifying spatial position of the graphene nanoinclusion are presented in Figs. 3b and 4b. With these dependences, a longer GB fragment migrates over a larger distance, as compared to a shorter GB fragment. In the partial case where the nanoinclusion is located exactly at the GB AD center, the migration distances l_{e1} and l_{e2} are identical. Figs. 3c and 4c shows dependences of l_{e1} and l_{e2} on the half-length a of the graphene nanoinclusion. From this figure it follows that the migration distances diminish when a increases. That is, longer inclusions more effectively hamper stress-driven GB migration than their shorter counterparts.

Comparison of dependences presented in Figs. 3 and 4 shows that they are very similar, despite of large difference in both elastic constants and the specific GB energy between Al and Ni. The reason for the similarity can be understood from analysis of formulas (1)–(4). As to details, is the elastic energy part of ΔW is expressed in units of $D\omega^2d^2$, and the applied shear stress is expressed in units of

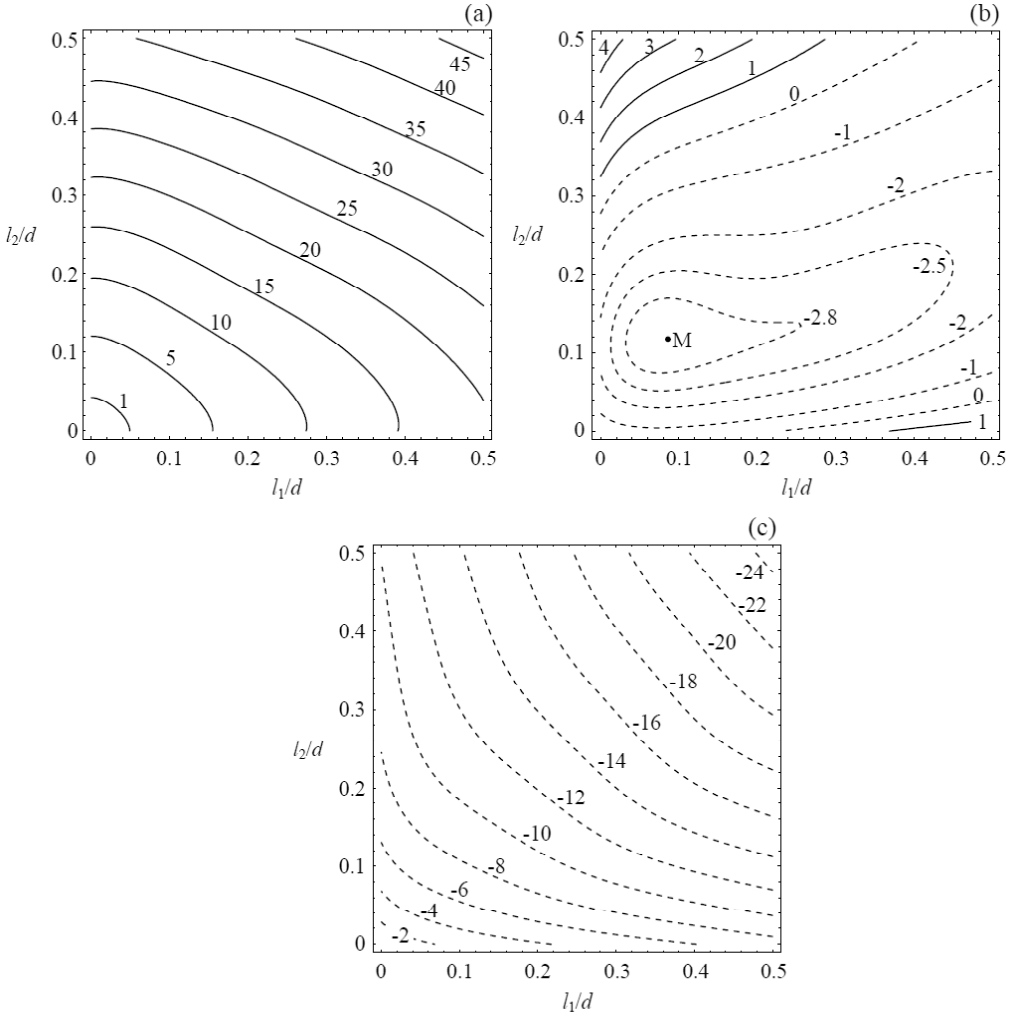

Fig. 2. Maps of the energy change ΔW depending the migration distances l_1 and l_2 in Al-graphene nanocomposite, for d=50 nm, ω=0.5, h=0.4d, a=0.1d and various values of the applied shear stress: (a) τ=0.01$D\omega$, (b) τ=0.6$D\omega$, and (c) τ=0.9$D\omega$. The energy change levels in the maps are shown in units of $10^{-2}D\omega^2d^2/2$.

$D\omega$, one finds that the energy change ΔW is sensitive to only one material parameter, namely the ratio γ/D. For various conventional metals, this ratio has similar values. For example, the ratio γ/D for Ni is 1.4 times larger than that for Al. This explains the similarity of dependences presented in Figs. 3 and 4.

The critical stresses τ_{c1} and τ_{c2} for the migration onset and transition to the unstable migration regime, respectively, serve as important characteristics of stress-driven GB migration. The critical stress τ_{c1} is defined as the minimum stress at which the migration onset is energetically favorable. More precisely, τ_{c1} is defined as the minimum stress at which one of the equilibrium migration distances (l_{e1} or l_{e2}) achieves some characteristic minimum value (denoted as b) allowing one to experimentally identify the fact that GB migrates. We take b as a GB width, that is, to a good approximation we have: b=1 nm. After numerical analysis of the calculated dependences (Figs. 3 and 4), we find typical values of τ_{c1}. For instance, in Al-graphene nanocomposite, for ω=0.5, a=0.1d, h=0.5d and various GB lengths (being close to grain sizes) d=50, 100, and 200 nm, we obtain: $\tau_{c1}\approx$ 849, 524, and 312 MPa, respectively. For comparison, in paper [20], it was found that the critical stress for the migration onset in pure metal without inclusions is given as: $\tau'_{c1}=D\omega(b/d)\ln(d/b)$. For the same values of parameters in pure Al, we have $\tau'_{c1}\approx$ 250, 147, and 85 MPa. In the case of Ni-graphene nanocomposite, for the same values of parameters as above, we find: $\tau_{c1}\approx$ 2.37, 1.46, and 0.87 GPa. In the case of pure Ni, we have $\tau'_{c1}\approx$ 685, 403, and 232 MPa. Thus, values of the critical stress τ_{c1} for the migration onset in Al-graphene and

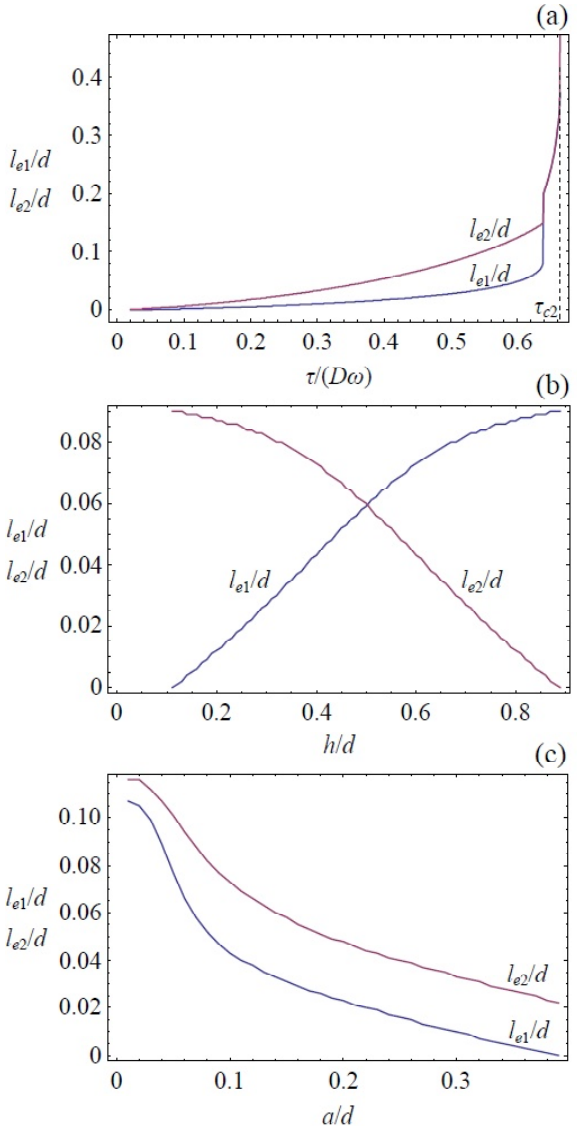

Fig. 3. Dependences of the equilibrium migration distances in Al-graphene nanocomposite, calculated at d=50 nm and ω=0.5, on (a) the applied shear stress τ, for h=0.3d, and a=0.1d; (b) parameter h, for τ=0.5$D\omega$ and a=0.1d; and (c) inclusion half-length a, for τ=0.5$D\omega$ and h=0.4d.

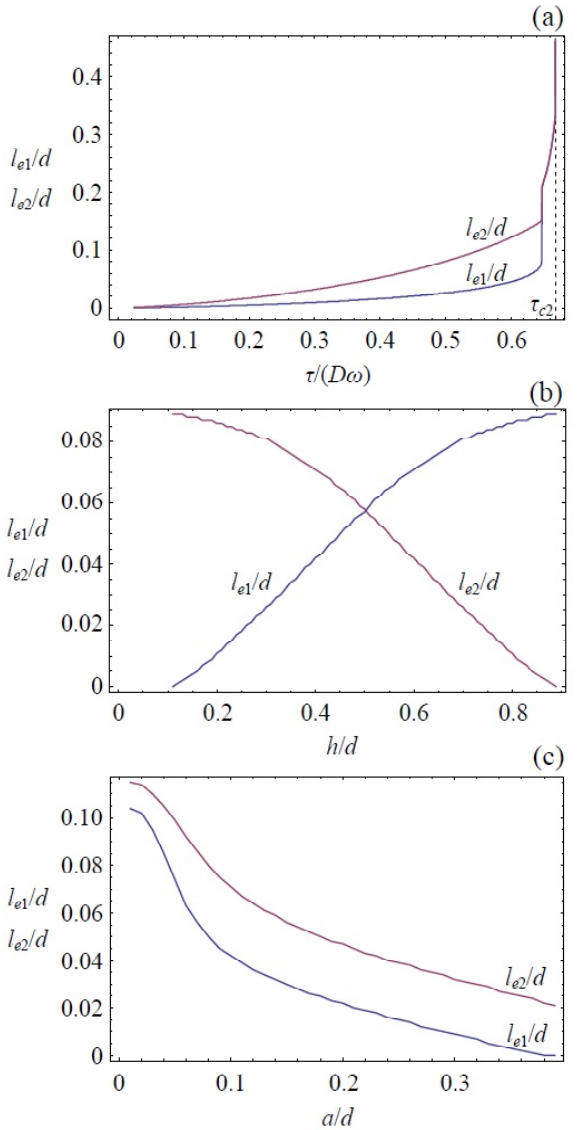

Fig. 4. Dependences of the equilibrium migration distances in Ni-graphene composite, calculated at d=50 mm and ω=0.5, on (a) the applied shear stress τ, for h=0.3d and a=0.1d; (b) parameter h, for τ=0.5$D\omega$ and a=0.1d; and (c) inclusion half-length a, for τ=0.5$D\omega$ and h=0.4d.

Ni-graphene nanocomposites is significantly larger than those of the stress τ'_{c1} in unreinforced Al and Ni. At the same time, values of the critical stress τ_{c1} are rather realistic. They can be achieved in conventional quasistatic deformation regimes so that stress-driven GB migration can effectively contribute to plastic flow in metal-graphene nanocomposites. If it is so, with comparatively high values of the critical stress τ_{c1}, one concludes that graphene nanoinclusions make metal-graphene nanocomposites stronger as compared to pure metals. This theoretical conclusion is well consistent with experimental data reported in the literature; see review [58] and references therein.

We now numerically estimate the critical stress τ_{c2} specifying transition to the unstable migration regime. Estimation results are presented in Figs. 5 and 6, for Al-graphene and Ni-graphene composites, respectively. In particular, Figures 5a and 6a demonstrate dependences of $\tau_{c2}(a)$ for ω=0.5, h/d=0.2, 0.3, 0.4, 0.5, and d=50 nm. For comparison, following [20], the critical stress for the un-

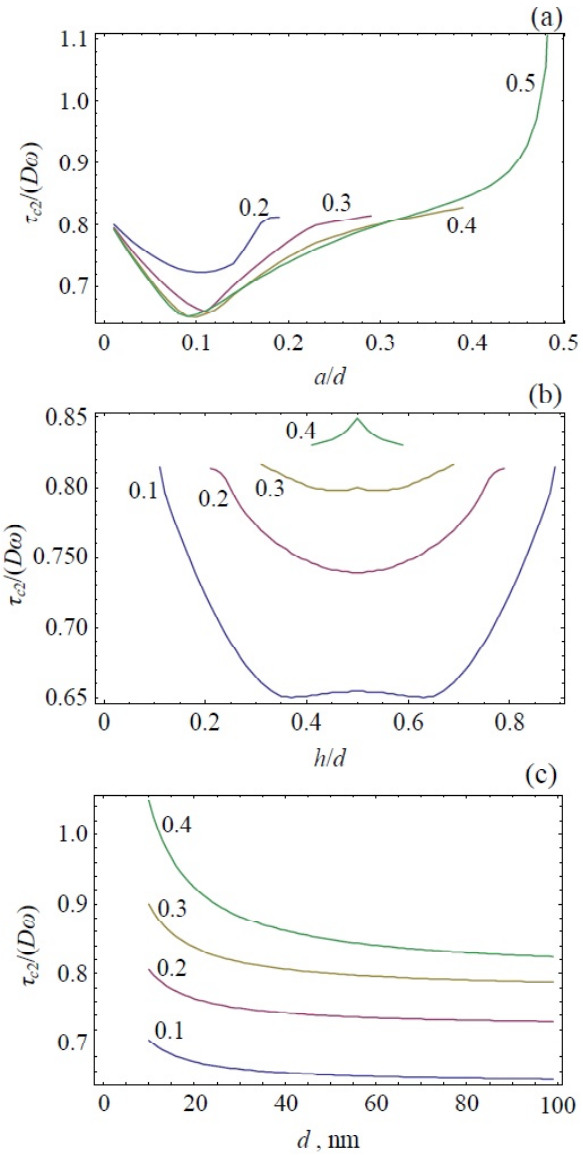

Fig. 5. Dependences of the critical shear stress τ_{c2} in Al-graphene nanocomposite, calculated for ω=0.5 on (a) inclusion half-length *a*, for *d*=50 nm and various values of parameter *h* (these values are shown in units of *d* near corresponding curves); (b) parameter *h*, for *d*=50 nm and various values of inclusion half-length *a* (these values are shown in units of *d* near corresponding curves); (c) and grain boundary length (close to grain size) *d*, for *h*=0.5 and various values of inclusion half-length *a* (these values are shown in units of *d* near corresponding curves).

stable migration in pure metal (without inclusions) is given as $\tau'_{c2} \approx 0.8D\omega$. As it follows from Figs. 5a and 6a, the inequality $\tau_{c2} < \tau'_{c2}$ holds in a wide range of nanoinclusion sizes (a<0.2-0.3d, depending on parameter *h*) in Al-graphene and Ni-graphene nanocomposites. That is, transition to the unstable migration in Al-graphene nanocomposites is enhanced as compared to that in pure metals. From a physical viewpoint, this is related to the fact that the defect configuration shown in Fig. 1c in the discussed range of nanoinclusion lengths due to the effective mutual screening of stress fields created by the disclination quadrupoles quadrupoles AA'B'B and CC'D'D has lower energy than that examined in the model [20] in the case of unreinforced metals.

The unstable migration serves as the dominant mechanism for grain growth in mechanically treated metals. In this context, our theoretical analysis shows that grain growth is enhanced in plastically deformed Al-graphene and Ni-graphene nanocomposites with relatively "short" graphene nanoplatelets specified by lengths 2a<0.4-0.6d, as compared to pure metals. At the same time, in the case of "long" graphene nanoinclusions with 2a>0.4-0.6d, the critical stress for the unstable migration satisfy the inequality $\tau_{c2} > \tau'_{c2}$ so that grain growth is hampered in Al- and Ni-graphene nanocomposites as compared to pure Al and Ni.

Note that our previous model [64] based on the assumption that the GB fragments A'B' and C'D' synchronously migrate over the same distance predicts the unstable migration to be always hampered in metal-graphene nanocomposites as compared to that in unreinforced metals. In contrast, the current theoretical examination (taking into account a realistic situation where the GB fragments A'B' and C'D' can migrate over different distances) predicts that graphene inclusions either hamper or enhance stress-driven GB migration, depending on inclusion length.

Also, note that each of the dependences $\tau_{c2}(a)$ has its pronounced minimum at $a \approx 0.1d$ (Figs. 5a and 6a). That is, GBs with graphene nanoinclusions specified by $a \approx 0.1d$ show the tendency to easily migrate under stress.

Figs. 5b and 6b present dependences $\tau_{c2}(h)$ calculated for ω=0.5, various values of a/d=0.1, 0.2, 0.3, 0.4, and d=50 nm. It is seen that dependences $\tau_{c2}(h)$ are significantly sensitive to the graphene nanoplatelet length. Indeed, for comparatively short nanoinclusions, each of the dependences $\tau_{c2}(h)$ has minimums near h=0.5. In other terms, the critical stress for the unstable migration is minimal, when the graphene nanoinclusion is located close to the middle of the migrating GB. For comparatively long nanoinclusions we have the opposite situation: the dependence $\tau_{c2}(h)$ has its maximum at h=0.5. This is explained by the fact that transition to the unstable migration is enhanced in a non-linear manner with rising the graphene nanoinclusion length. For instance, when a long nanoinclusion (with a

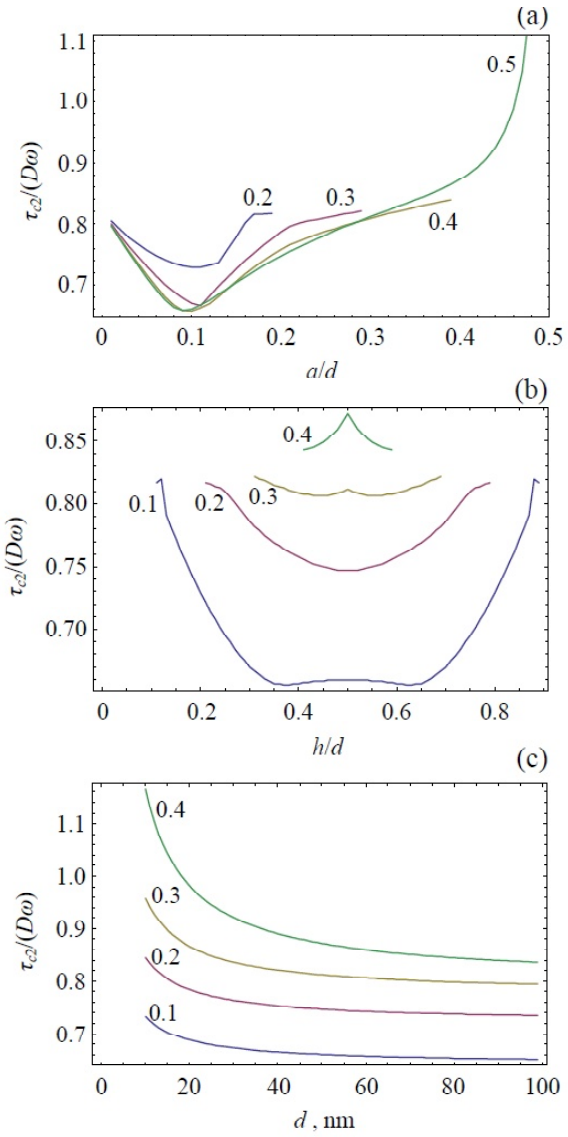

Fig. 6. Dependences of the critical shear stress τ_{c2} in Ni-graphene nanocomposite, calculated for ω=0.5 on (a) inclusion half-length *a*, for *d*=50 nm and various values of parameter *h* (these values are shown in units of *d* near corresponding curves); (b) parameter *h*, for *d*=50 nm and various values of inclusion half-length *a* (these values are shown in units of *d* near corresponding curves); (c) and grain boundary length (close to grain size) *d*, for *h*=0.5 and various values of inclusion half-length *a* (these values are shown in units of *d* near corresponding curves).

length exceeding a half-length of the GB AD) is located at the GB AD middle, both migrating GB fragments are short enough so that the critical stress τ_{c2} is high. However, when the nanoinclusion is shifted closer to GB junction A or D, one of the migrating GB fragments becomes long, in which case the critical stress τ_{c2} for its unstable migration significantly decreases.

Figs. 5c and 6c present dependences $\tau_{c2}(d)$ calculated for ω=0.5, *h*=0.5, and various values of *a*/*d*=0.1, 0.2, 0.3 and 0.4. It is seen that critical stress τ_{c2} significantly grows with decreasing grain size. Thus, in nanocomposites characterized by extremely small grain sizes, the unstable migration is hampered (compared to pure metals) in all range of nanoinclusion parameters.

Comparison of dependences presented in Figs. 5 and 6 shows that the difference in the critical stress τ_{c2} (expressed in units of $D\omega$) between Al- and Ni-graphene nanocomposites is very small. Typically, the difference ~1–2%; although it reaches 10% in the case of ultra-small GB lengths. As with the migration distances (Figs. 3 and 4), the small difference in the critical stress τ_{c2} between Al- and Ni-graphene nanocomposites is explained by the sensitivity of the energy change ΔW to only one material parameter, the ratio γ/D. For various conventional metals, this ratio has similar values.

However, one can distinguish Gum metal [70-73] as a metallic material having the ratio γ/D whose value is significantly different from those of conventional metals. Gum metals are special titanium alloys exhibiting the unique mechanical properties, including very low shear modulus G [70-73]. In our simulations, we will use *G* ~15 GPa and ν =0.3 [71]. The GB energy in Gum metals is unknown, in which case we will take its value of γ =1 J/m^2 which is typical for pure titanium [74]. In doing so, for Gum metal, we find the ratio γ/D to be approximately 4.7 and 3.2 times larger than its counterparts in Al and Ni, respectively. Note that Gum metals represent coarse-grained polycrystalline metals with grain sizes being tens of microns [70-73]. Nevertheless, for the aims of this paper, we will examine the critical stress τ_{c2} for the unstable GB migration in Gum metal with nanoscale grains and compare it with values of τ_{c2} in nanostructured Al and Ni in order to understand the effect of g/*D* on stress-driven grain growth in meals. Fig. 7 presents the dependences which are calculated for Gum metal in the same way as those in Figs. 5 and 6, calculated for Al and Ni, respectively. From Figs. 5-7 it follows that values of τ_{c2} (in units of $D\omega$) for Gum-metal-graphene nanocomposites are higher than those for Al- and Ni-graphene nanocomposites with the same GB length and characteristics of graphene nanoionclusions. This difference in τ_{c2} due to the effect of the ratio γ/D is especially significant (~90%) at very small GB lengths (~10 nm) and less pronounced (~10-25%) at larger GB lengths (~50-100 nm).

To generalize the obtained results, we may logically conclude that stress-driven grain growth in metal-graphene nanocomposites is either enhanced or hampered by graphene nanoinclusions, depending on their typical length and GB length (grain size). The hampering effect exerted by graphene nanoinclusions on stress-driven grain growth enhances with rising the ratio γ/D specifying metal matrix in a metal-graphene nanocomposite.

4. CONCLUDING REMARKS

Thus, we theoretically described stress-driven GB migration in metal-graphene nanocomposites. In the framework of our description, stress-driven migration of high-angle GBs gives rise to the formation of both new GB fragments and wedge disclinations at GB junctions and edges of graphene inclusions. The new GB fragments and disclinations cause the main hampering force for the migration process.

Energy and stress characteristics of stress-driven GB migration in metal-graphene nanocomposites are calculated. In particular, we revealed that the critical stress τ_{c1} for the migration onset in Al-graphene and Ni-graphene nanocomposites is significantly larger than its counterpart τ'_{c1} in reinforced Al and Ni. At the same time, values of the critical stress τ_{c1} are rather realistic. They can be achieved in conventional quasistatic deformation regimes so that stress-driven GB migration can effectively contribute to plastic flow in Al-graphene nanocomposite. If it is so, with comparatively high values of the critical stress τ_{c1}, one concludes that graphene nanoinclusions make Al-graphene nanocomposites stronger as compared to pure Al. This theoretical conclusion is well consistent with experimental data reported in literature (for a review, see [58]).

Also, it is revealed that stress-driven grain growth in metal-graphene nanocomposites is either enhanced or hampered by graphene nanoinclusions, when they are long or short, respectively. The hampering effect exerted by graphene nanoinclusions on stress-driven grain growth enhances with rising the ratio γ/D specifying metal matrix in a metal-graphene nanocomposite.

These theoretical results are of utmost interest for synthesis of metal-graphene nanomposites with controlled microstructure and enhanced strength. In particular, fabrication of metal-matrix nanocomposites containing “long” graphene nanoinclusions will allow one to stabilize grain size in metal matrix and thus control its strength contributing to strength characteristics of nanocomposites.

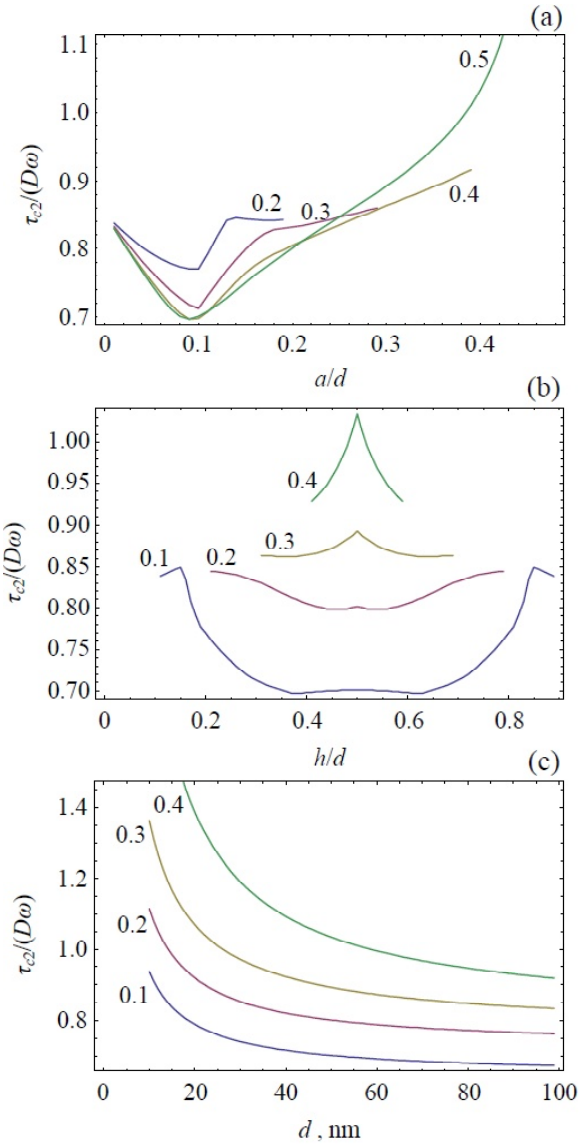

Fig. 7. Dependences of the critical shear stress τ_{c2} in Gum-metal-graphene nanocomposite, calculated for ω=0.5 on (a) inclusion half-length *a*, for *d*=50 nm and various values of parameter *h* (these values are shown in units of *d* near corresponding curves); (b) parameter *h*, for *d*=50 nm and various values of inclusion half-length *a* (these values are shown in units of *d* near corresponding curves); (c) and grain boundary length (close to grain size) *d*, for *h*=0.5 and various values of inclusion half-length *a* (these values are shown in units of *d* near corresponding curves).

ACKNOWLEDGEMENTS

This work was supported, in part (for SVB), by the Council for grants of the President of Russian Federation (grant MD-3154.2017.1) and, in part (for NFM and IAO), by the Russian Ministry of Education and Science (Zadanie 9.1964.2014/K).

REFERENCES

[1] K.S. Kumar, S. Suresh and H. Van Swygenhoven // *Acta Mater*. **51** (2003) 5743.
[2] I.A. Ovid'ko // *Int. Mater. Rev*. **50** (2005) 65.
[3] D. Wolf, V. Yamakov, S.R. Phillpot, A.K. Mukherjee and H. Gleiter // *Acta Mater*. **53** (2005) 1.
[4] M.A. Meyers, A. Mishra and D.J. Benson // *Prog. Mater. Sci.* **51** (2006) 427.
[5] C.C. Koch, I.A. Ovid'ko, S. Seal and S. Veprek, *Structural Nanocrystalline Materials: Fundamentals and Applications* (Cambridge University Press, Cambridge, 2007).
[6] M. Dao, L. Lu, R.J. Asaro, J.T.M. De Hosson and E. Ma // *Acta Mater*. **55** (2007) 4041.
[7] C.S. Pande and K.P. Cooper // *Prog. Mater. Sci.* **54** (2009) 689.
[8] E.C. Aifantis // *Mater. Sci. Eng. A* **503** (2009) 190.
[9] *Bulk Nanostructured Materials*, ed. by M.J. Zehetbauer and Y.T. Zhu (Wiley, Weinhein, 2009).
[10] J.R. Greer and J.T.M. De Hosson // *Prog. Mater. Sci.* **56** (2011) 654.
[11] I.A. Ovid'ko and T.G. Langdon // *Rev. Adv. Mater. Sci.* **30** (2012) 103.
[12] Y.T. Zhu, X.Z. Liao and X.-L. Wu // *Prog. Mater. Sci.* **57** (2012) 1.
[13] R.Z. Valiev, A.P. Zhilyaev and T.G. Langdon, *Bulk Nanostructured Materials: Fundamentals and Applications* (Wiley, Hoboken, New Jersey, 2014).
[14] R.W. Armstrong // *Mater. Trans.* **55** (2014) 2–12.
[15] R.Z. Valiev and Y.T. Zhu // *Trans. MRS Japan* **40** (2015) 309.
[16] P. Kumar, M. Kawasaki and T.G. Langdon // *J. Mater. Sci.* **51** (2016) 7–18.
[17] M. Kawasaki and T.G. Langdon // *J. Mater. Sci.* **51** (2016) 19.
[18] M. Jin, A.M. Minor, E.A. Stach and J.W. Morris Jr. // *Acta Mater.* **52** (2004) 5381.
[19] W.A. Soer, J.T.M. De Hosson, A.M. Minor, J.W. Morris Jr. and E.A. Stach // *Acta Mater.* **52** (2004) 5783–5790.
[20] M.Yu. Gutkin and I.A. Ovid'ko // *Appl. Phys. Lett.* **87** (2005) 251916.
[21] F. Sansoz and V. Dupont // *Appl. Phys. Lett.* **89** (2006) 111901.
[22] D. Farkas, A. Froseth and H. Van Swygenhoven // *Scr. Mater.* **55** (2006) 695.
[23] J.T.M. De Hosson, W.A. Soer, A.M. Minor, Z. Shan, E.A. Stach, S.A. Syed Asif and O.L. Warren // *J. Mater. Sci.* **41** (2006) 7704.
[24] D.S. Gianola, S. Van Petegem, M. Legros, S. Brandstetter, H. Van Swygenhoven and K.J. Hemker // *Acta Mater.* **54** (2006) 2253.
[25] D.S. Gianola, D.H. Warner, J.F. Molinari and K.J. Hemker // *Scr. Mater.* **55** (2006) 649.
[26] X.Z. Liao, A.R. Kilmametov, R.Z. Valiev, H. Gao, X. Li, A.K. Mukherjee, J.F. Bingert and Y.T. Zhu // *Appl. Phys. Lett.* **88** (2006) 021909.
[27] P.L. Gai, K. Zhang and J. Weertman // *Scr. Mater.* **56** (2007) 25.
[28] D. Pan, S. Kuwano, T. Fujita and M.W. Chen // *Nano Lett.* **7** (2007) 2108.
[29] V. Dupont and F. Sansoz // *Acta Mater.* **56** (2008) 6013.
[30] I.A. Ovid'ko, A.G. Sheinerman and E.C. Aifantis // *Acta Mater.* **56** (2008) 2718.
[31] T.J. Rupert, D.S. Gianola, Y. Gan and K.J. Hemker // Science **326** (2009) 1686.
[32] S. Cheng, Y. Zhao, Y. Wang, Y. Li, X.-L. Wang, P.K. Liaw and E.J. Lavernia // *Phys. Rev. Lett.* **104** (2010) 255501.
[33] S.V. Bobylev, N.F. Morozov and I.A. Ovid'ko // *Phys. Rev. Lett.* **105** (2010) 055504.
[34] S.V. Bobylev, N.F. Morozov and I.A. Ovid'ko // *Phys. Rev. B* **84** (2011) 094103.
[35] J.A. Sharon, P.-C. Su, F.B. Prinz and K.J. Hemker // *Scr. Mater.* **64** (2011) 25.
[36] D.S. Gianola, D. Farkas, M. Gamarra and M. He // *J. Appl. Phys.* **112** (2012) 124313.
[37] S.V. Bobylev and I.A. Ovid'ko // *Phys. Rev. Lett.* **109** (2012) 175501.
[38] H. Feng, Q.H. Fang, L.C. Zhang and Y.W. Liu // *Mech. Mater.* **61** (2013) 39.
[39] M. Yu, Q.H. Fang, H. Feng and Y.W. Liu // *Acta Mech.* **225** (2014) 2005.
[40] Y. Zhao, Q. Fang and Y. Liu // *Philos. Mag.* **94** (2014) 700.
[41] Y. Lin, H. Wen, Y. Li, B. Wen and E.J. Lavernia // *Metall. Mater. Trans. B* **45** (2014) 795.
[42] Y. Lin, B. Xu, Y. Feng and E.J. Lavernia // *J. Alloys Comp.* **596** (2014) 79.
[43] Y. Lin, H. Wen, Y. Li, B. Wen, L. Wei and E.J. Lavernia // *Acta Mater.* **82** (2015) 304.
[44] I.A. Ovid'ko and A.G. Sheinerman // *J. Mater. Sci.* **50** (2015) 4430.
[45] S.V. Bobylev and I.A. Ovid'ko // *Acta Mater.* **88** (2015) 260.

[46] I.A. Ovid'ko and A.G. Sheinerman // *Acta Mater.* **121** (2016) 117.
[47] S.V. Bobylev and I.A. Ovid'ko // *Acta Mater.* **124** (2017) 333.
[48] C. Lee, X. Wei, J.W. Kysar and J. Hone // *Science* **321** (2008) 385.
[49] I.A. Ovid'ko // *Rev. Adv. Mater. Sci.* **34** (2013) 1.
[50] C. Daniels, A. Horning, A. Phillips, D.V.P. Massote, L. Liang, Z. Bullard, B.G. Sumpter and V. Meunier // *J. Phys.: Condens. Matter* **27** (2015) 373002.
[51] J. Wang, Z. Li, G. Fan, H. Pan, Z. Chen and D. Zhang // *Scr. Mater*. **66** (2012) 594.
[52] L.-Y. Chen, H. Konishi, A. Fehrenbacher, C. Ma, G.-Q Hu, H. Choi, H.-F. Hu, F.E. Pfefferkorn and X.-C. Li // *Scr.Mater*. **67** (2012) 29.
[53] A.G. Nasibulin, T.S. Koltsova, L.I. Nasibulina, I.V. Anoshkin, A. Semencha, O.V. Tolochko and E.I. Kauppinen // *Acta Mater.* **61** (2013) 1862.
[54] Y. Kim, J. Lee, M.S. Yeom, J.W. Shin, H. Kim, Y. Cui, J.W. Kysar, J. Hone, Y. Jung, S. Jeon and S.M. Yan // *Nature Commun.* **4** (2013) 2114.
[55] J. Hwang, T. Yoon, S.Y. Jin, J. Lee, T.-S. Kim, S.H. Hong and S. Jeon // *Adv. Mater.* **25** (2013) 6724.
[56] D. Kuang, L. Xu, L. Liu, W. Hu and Y. Wu // *Appl. Surf. Sci.* **273** (2013) 484.
[57]C.L.P. Pavithra, B.V. Sarada, K.V. Rajulapoti, T.N. Rao and D. Sundararajan // *Sci. Rep.* **4** (2014) 4049.
[58] I.A. Ovidko // *Rev. Adv. Mater. Sci.* **38** (2014) 190.
[59] H. Algul, M. Tokur, S. Ozcan, M. Uysal, T. Cetinkaya, H. Akbulut and A. Alp // *App. Surf. Sci.* **359** (2015) 340.
[60] V.G. Konakov, O.Yu. Kurapova, I.V. Lomakin, I.Yu. Archakov, E.N. Solovyeva and I.A. Ovidko // *Rev. Adv. Mater. Sci.* **44** (2016) 361.
[61] D. Zhang and Z. Zhan // *J. Alloys Comp.* **654** (2016) 226; **658** (2016) 663.
[62] S. N. Alam and L. Kumar // *Mater. Sci. Eng. A* **667** (2016) 16.
[63] O.Yu. Kurapova, V.G. Konakov, A.S. Grashchenko, N.N. Novik, S.N. Golubev and I.A. Ovid'ko // *Rev. Adv. Mater. Sci.* **48** (2017) 89.
[64] S.V. Bobylev, N.F. Morozov and I.A. Ovid'ko // *Dokl. Phys.* (2017) in press.
[65] A.E. Romanov, V.I. Vladimirov, In: *Dislocations in solids*, vol. 9, ed. by F.R.N. Nabarro (NorthHolland,Amsterdam, 1992), p. 191.
[66] J.P. Hirth and J. Lothe, *Theory of Dislocations* (Wiley, New York, 1982).
[67] A.P. Sutton and R.W. Balluffi // *Acta Metall.* **35** (1987) 2177.
[68] A.P. Sutton and R.W. Balluffi, *Interfaces in Crystalline Materials* (Oxford Science Publications, Oxford, 1996).
[69] H. Van Swygenhoven, D. Farkas and A. Caro // *Phys. Rev. B* **62** (2000) 831.
[70] T. Saito, T. Furuta, J.-H. Hwang, S. Kuramoto, K. Nishino, N. Suzuki, R. Chen, A. Yamada, K. Ito, Y. Seno, T. Nonaka, H. Ikehata, N. Nagasako, C. Iwamoto, Y. Ikuhara and T. Sakuma // *Science* **300** (2003) 464.
[71] S. Kuramoto, T. Furuta, J.-H. Hwang, K. Nishino and T. Saito // *Met. Mater. Trans. A* **37** (2006) 657.
[72] M.Yu. Gutkin, T. Ishizaki, S. Kuramoto and I.A. Ovid'ko // *Acta Mater.* **54** (2006) 2489.
[73] T. Furuta, S. Kuramoto, J.W. Morris, Jr., N. Nagasako, E. Withey and D.C. Chrzan // *Scr. Mater*. **68** (2013) 767.
[74] C.C. Camilo, E.C. Souza, P.L. Di Lorenzo and J.M.D.A. Rollo // *Braz. J. Biom. Eng.* **27** (2011) 175.